Chemical Engineering Journal 259 (2015) 865–875

Contents lists available at ScienceDirect

Chemical Engineering Journal

journal homepage: www.elsevier.com/locate/cej

Reactive adsorption of pharmaceuticals on tin oxide pillared montmorillonite: Effect of visible light exposure

Carla B. Vidal [a,b], André B. dos Santos [b], Ronaldo F. do Nascimento [c], Teresa J. Bandosz [a,*]

[a] Department of Chemistry, The City College of New York and the Graduate School of the City University of New York, 160 Convent Avenue, New York, NY 10031, USA
[b] Department of Hydraulic and Environmental Engineering, Federal University of Ceará, Rua do Contorno, S/N Campus do Pici, Bl. 713, CEP: 60451-970 Fortaleza, CE, Brazil
[c] Department of Analytical Chemistry and Physical Chemistry, Federal University of Ceará, Rua do Contorno, S/N Campus do Pici, Bl. 940, CEP: 60451-970 Fortaleza, CE, Brazil

HIGHLIGHTS

- Montmorillonite was pillared with tin oxide.
- As increase in the surface area was found owing to the deposition of SnO_2.
- The pillared clay was used for adsorption of trimethoprim and sulfamethoxazole.
- As increase in the adsorption was found compared to the initial clay.
- Solar light decomposes trimethoprim and thus increases its adsorption in small pores.

GRAPHICAL ABSTRACT

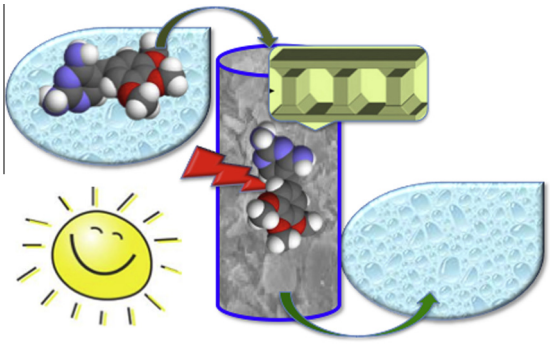

ARTICLE INFO

Article history:
Received 3 June 2014
Received in revised form 15 July 2014
Accepted 16 July 2014
Available online 9 August 2014

Keywords:
Adsorption
Pharmaceuticals
Pillared clay
Tin oxide

ABSTRACT

Montmorillonite (Mt) clay was pillared with SnO_2 and tested as an adsorbent for the removal pharmaceuticals trimethoprim (TMP) and sulfamethoxazole (SMX) frequently present in wastewaters. Adsorption process was carried out in dynamic conditions and the effects of light exposure were investigated. The initial and modified clays were characterized using XRD, FTIR, SEM, potentiometric titration, TA/MS and adsorption of nitrogen. The XRD analysis revealed an enlargement of the clay's interlayer space as a consequence of SnO_2 particles intercalation into the clay interlayer spaces. A marked increase in the volume of mesopores was also noticed. It indicated the precipitation of tin species on the flake surface. These changes resulted in a five-fold increase in TMP adsorption. Upon exposure to light a 30% increase in TMP adsorption was found in comparison to the performance in the dark. The good performance of the modified clay was linked to specific acid–base and electrostatic interactions of TMP with the Lewis acid sites of SnO_2. Since exposure to solar light resulted in the decomposition of some TMP adsorbed on the surface, those smaller molecules formed were able to relocate to small pores of higher adsorption energy, which were initially inaccessible for TMP. SMX was not adsorbed on the surface of the modified clay owing mainly to its acidic character.

1. Introduction

The presence of pharmaceuticals and their metabolites in water have caught global attention due to its environmental and health hazards [1]. Among the various types of pollutants, pharmaceuticals are of particular concern because they can interfere with the function of the endocrine system in wildlife and humans [2]. The majority of pharmaceuticals that has been reported as dangerous to living organisms can be found in municipal wastewater. These compounds usually are not completely removed by conventional wastewater treatment due to their high resistance

* Corresponding author. Tel.: +1 (212)650 6077; fax: +1 (212)650 6107.
E-mail address: tbandosz@ccny.cuny.edu (T.J. Bandosz).

http://dx.doi.org/10.1016/j.cej.2014.07.079
1385-8947/

to biodegradation [3,4]. Moreover, various pharmaceuticals have been also detected in seawater. Their presence in such ecosystems is attributed to the transport of contaminated wastewater effluents by rivers into larger water bodies such as oceans and seas, which indicates that they can be quite persistent to natural biotransformation [5]. To reduce the potential risk caused by these compounds in treated wastewater discharged to aquatic environments, their removal in water treatment plants is considered as an important technological challenge.

Adsorption is one of the most promising techniques used to remove pharmaceuticals from water [4]. Among the adsorbents used for water decontamination clay minerals are often selected, owing to their low cost and selectivity to adsorb specific contaminants [6–8].

Montmorillonite (Mt) is an abundant clay mineral, consisting of two layers of tetrahedral silica sheets sandwiching one octahedral alumina sheet [9]. Its interlayer charge is neutralized by the presence of cations such as sodium or calcium. The cationic layered clays can be transformed into highly porous structures by a three-step synthesis procedure: (1) polymerization of a multivalent cation (such as Al^{3+}, Ga^{3+}, Ti^{4+}, Zr^{4+}, Sn^{+4}, Fe^{3+}, and Cr^{3+}, among others) leading to polycations; (2) intercalation of these hydroxy-metal polycations into the interlayer space of clays, involving the substitution of natural exchangeable charge-compensating cations; and (3) calcination at moderate temperatures [10,11]. The latter step is necessary because the solids obtained after the second step, usually called intercalated clays, are metastable, like the polycations themselves. Calcination transforms the polycations into stable oxy-hydroxide phases referred to as pillars, which contribute significantly to the porosity development in such materials [12].

Over the past few years various nanostructures of tin oxide such as nano-wire, nano-tubes, nano-rods, nano-sheets, nano-particles and nano-pillars have been reported with their diversifying properties and, hence, functionalities [13–15]. Even though tin oxide has been studied as an adsorbent from a gas phase [16–18], there are few studies in the literature using it in the clay pillaring process [13,19–21] or analyzing in details its beneficial effects for the separation of pollutants.

Tin oxide exists in two different forms; as stannous oxide/tin monoxide (SnO) and as stannic oxide/tin dioxide (SnO_2). The existence of these two oxides reflects the dual valency of tin with valence states of 2^+ and 4^+, respectively. During the pillaring processes SnO is easily oxidized to SnO_2 [21,22].

SnO_2 is a well-known semiconductor oxide, which has received considerable attention due to its photocatalytic properties in the degradation of organic pollutants [23,24]. Wang and co-workers [25] synthesized and studied the photocatalytic properties of mesoporous SnO_2–hexaniobate layered nanocomposites and they found that the nanocomposite demonstrates a high photocatalytic activity in the degradation of acid red G under UV-light irradiation, which can be ascribed to its high surface area, mesoporosity and the synergistic effect of the two components (SnO_2 and hexaniobate). Bandara and co-workers [26] studied composites of tin and zinc oxide nanocrystalline particles for enhanced charge separation in sensitized degradation of dyes. Improved photocatalytic activity was observed in the case of ZnO/SnO_2 composite catalyst compared to the catalytic activity of ZnO, SnO_2 or TiO_2 powder. A novel preparation method for nanosized ZnO–SnO_2 with high photocatalytic activity for methyl orange by homogeneous co-precipitation was proposed by Zhang and co-workers [27]. Fresno and co-workers [28] compared the photocatalytic activity of Sn-doped TiO_2 with P25 TiO_2 for the degradation of chlorsulfuron (ChS). Their results showed a beneficial effect of the presence of Sn^{4+} in the TiO_2 lattice. Bisphenol photodegradation on nanoporous SnO_2 and TiO_2 was investigated by Kim and co-workers [29] who also found an improvement when two materials were combined.

Based on the above, the objective of this paper is to investigate the effect of SnO_2 treatment on the properties of a montmorillonite from Brazil and to evaluate the modified montmorillonite as an adsorbent/reactive adsorbent for the removal of TMP and SMX frequently present in raw and treated wastewaters. We focus on the examination of the effect of the tin species surface location on the adsorption and photodegradation processes. To derive the mechanism of surface interactions and elucidate the role of tin oxide in the separation process. An extensive characterization of the initial clay, its tin oxide modified counterpart and the exhausted samples with TMP and SMX has been carried out. Finally, adsorption experiments were conducted in light and in dark conditions in order to investigate the photoactivity effect.

2. Materials and methods

2.1. Materials/adsorbents

Montmorillonite (Mt) was supplied by Bentonisa (Campina Grande, Brazil). Its cation exchange capacity (CEC) is 0.108 mol/100 g. It was estimated using the ammonium acetate method [30].

The pillaring agent was prepared by adding dropwise 50 mL of tin chloride, $SnCl_2{\cdot}2H_2O$ (II) 0.4 mol L^{-1} to 50 mL of 0.4 mol L^{-1} KOH with continuous steering at 70 °C. No precipitation was observed. The final pH was 2. Previous studies have shown that the trimer $Sn_3(OH)_4^{2+}$ is one of the predominant species when Sn(II) salts undergo hydrolysis under controlled conditions [21], but at that pH, the $SnOH^+$, $Sn_2(OH)_2^{2+}$ species are also expected in the solution. Hydra/Medusa Chemical Equilibrium Database and Plotting Software were used to predict the polycations present in the pillaring agent solution (Fig. 1S of Supplementary Information). Mt (5.0 g) was well dispersed in 400 mL of deionized and then 100 mL of pillaring agent was added into the clay suspension. The mixture reaction was stirred at 60 °C for 24 h. The resulting suspension was centrifuged and washed several times with deionized water, dried at 80 °C and calcined at 500 °C for 3 h. During this process in the presence of air oxidation of Sn^{2+} to Sn^{+4} is expected to take place [21,22]. The modified clay is referred to as SnO_2–Mt. The exhausted samples after adsorption have a name of a specific adsorbate added.

2.2. Adsorbates

The pharmaceuticals used, trimethoprim (TMP) and sulfamethoxazole (SMX), were purchased from VWR (USA). Then, working solutions for the adsorption tests were prepared by diluting the adsorbate in distilled water to a concentration of 10 mg L^{-1} using an ultrasonic cleaner (Brason 1510) to improve the dissolution of the compounds. The physicochemical properties for the pharmaceuticals selected are shown in Table 1. Their structural formulas are given below.

2.3. Methods

X-Ray powder diffraction (XRD) patterns were recorded at XRD diffractometer (Philips X'Pert X-Ray diffractometer) with a $Cu_{K\alpha}$ radiation for crystalline phase with a routine power of 1600 W (40 kV, 40 mA).

The X-Ray fluorescence spectra were obtained using a wavelength dispersive X-Ray fluorescence spectrometer (model ZMS Mini II, Rigaku).

Scanning electron microscopy (SEM) was performed on Zeiss Supra 55 instrument with a resolution of 5 nm at 30 kV. Analyses were performed on a sample powder previously dried. A sputter coating of a thin layer of gold was performed to avoid specimen charging.

Table 1
Physicochemical properties for the pharmaceuticals used as adsorbates.

Adsorbate	Molecular formula	M.W.[a] (g/mol)	Water solubility (mg/L)	$\log K_{ow}$[a]	pK_a
TMP	$C_{14}H_{18}N_4O_3$	290.3	400	0.91	(1) ~3.2 (2) 6.6–7.34
SMX	$C_{10}H_{11}N_3O_3S$	253.3	610	0.89	(1) 1.6–1.85 (2) 5.57–5.7

[a] M.W – molar weight; $\log K_{ow}$ – octanol water partition coefficient.

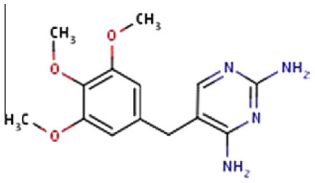

Trimethoprim

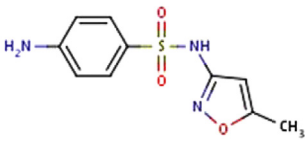

Sulfamethoxazole

FTIR spectroscopy was carried out on Nicolet Magna-IR 830 spectrometer using the attenuated total reflectance method (ATR). The spectrum was generated and collected 32 times and corrected for the background noise. The experiments were done on the powdered samples, without KBr addition.

Nitrogen isotherms were measured at −196 °C using an ASAP2020 instrument (Micromeritics). Prior to each measurement, the samples were outgassed at 120 °C to vacuum 4 mmHg. The surface area, S_{BET}, was calculated from the isotherms. The pore size distribution (PSD) was determined using the BJH method.

Thermogravimetric (TG) curves were measured on a TA thermal analyzer (SDT Q600), which was connected to a gas analysis MS system (OMNI Star). The samples were heated up to 1000 °C (10 °C min^{-1}) under a constant helium flow (100 mL min^{-1}). From the TG curves, DTG curves were derived. The composition of gases was evaluated using MS, and gas evolution profiles as a function of temperature were obtained.

Potentiometric titration measurements were performed with a DMS Titrino 716 automatic titrator (Metrohm). The instrument was set at the mode where the equilibrium pH is collected. Subsamples of the initial materials (~0.05 g) were added to $NaNO_3$ (0.01 M, 25 mL) and placed in a container maintained at 25 °C overnight for equilibrium. During the titration, to eliminate the influence of atmospheric CO_2, the suspension was continuously saturated with N_2. The suspension was stirred throughout the measurements. Volumetric standard NaOH (0.1 M) was used as the titrant. The experiments were done in the pH range of 3–10. Each sample was titrated with base after acidifying the sample suspension [31]. The experimental data was transformed into a proton binding curve, ϑ, representing the total amount of protonated sites, which is related to the pK_a distribution by the integral equation [32]. The solution of this equation was obtained using the numerical SAIEUS procedure [32,33] which applies regularization combined with non-negativity constraints. The validity of the potentiometric titration method in detection of the pK_a for model compounds was demonstrated by Jagiello and co-workers [32,33] and Contescu and co-workers [34].

2.4. Adsorption experiments

Adsorption process was carried out in dynamic conditions at ambient temperature and pressure. Adsorbents with particle sizes 0.425–0.212 mm were packed into 60 mm polyethylene column with 4 mm inside diameter. The height of bed was approximately 18 mm with weight of 0.3 g. 1 L TMP solution was passed through the column with an adsorbent from the top by a peristaltic pump (MasterFlex C/L) with initial concentration of 10 mg L^{-1} and flow rate of 0.6 mL min^{-1}. Effluent was collected periodically in 2 mL fractions every 40 min. The column with SnO_2–Mt was covered with black screen, completely blocking light access. In order to evaluate the SnO_2 photocatalytic properties in the dynamic process, the tests were also run in the column exposed to simulated solar light source. For this a Solar Light XPS-150 Xenon lamp with an ozone-free Xenon bulb was used. The duration of the adsorption experiments was 25 h.

Qualitative and quantitative analyses of effluent samples were carried out with the use of a Waters 2690 liquid chromatograph with a Waters 996 photodiode array detector, Lichrospher® RP-18 column (10 nm, 5 μm, 4.0 mm × 125 mm, EM Separations, Gibbstown, NJ), methanol/trifluoacetic acid (TFA) 0.1% as mobile phase. For TMP compound the analyses were carried out in an isocratic programmed: 45% TFA/55% Methanol. For SMX compound the analyses were carried out in an isocratic programmed: 35% TFA/65% Methanol. The flow was 1.0 mL min^{-1}. The column was thermostatted during analysis at 35 °C.

In a breakthrough curve, C_0 is the adsorbate concentration in the effluent and V_e is the effluent volume that percolates through the adsorbent. The breakpoint, chosen arbitrarily as C_b, occurs when the effluent concentration reaches 5% of the initial concentration C_0. The adsorbent achieves complete saturation, when the concentration C_x approaches C_0. The total effluent amount, V_b, is passed through the adsorbent until the breakpoint is reached [2,35]. The part between C_x (exhaustion point) and C_b (breakpoint) is called primary adsorption zone (PAZ) and the time needed to establish PAZ in the adsorbent is calculated by Eq. (1):

$$t_x = \frac{V_x}{F_m} \tag{1}$$

where t_x is the time to establish PAZ (min), F_m is the flow rate (mL min^{-1}) and V_x is the exhaustion volume (mL). The time required for movement of PAZ down the column is given by Eq. (2):

$$t_\sigma = \frac{(V_x - V_b)}{F_m} \tag{2}$$

where t_σ is the time required for movement of PAZ down the column (min) and V_b is the breakthrough volume (mL). Thus, for depth D of the adsorbent bed, the depth and time ratios are given by Eq. (3):

$$U = \frac{\delta}{D} = \frac{t_\delta}{(t_x - t_f)} \tag{3}$$

where δ is the length of PAZ (cm), D is the adsorbent bed depth (cm), t_f is the PAZ formation time. The time required to achieve PAZ is given by Eq. (4):

$$t_f = (1 - F)t_\delta \tag{4}$$

where F is the adsorbent fractional capacity in the adsorption zone characterized by solute adsorption from the solution under limiting conditions. The adsorbent fractional capacity is given by Eq. (5):

$$F = \int_{V_b}^{V} \frac{(C_0 - C)d_v}{C_0(V_x - V_b)} \tag{5}$$

The adsorbent saturation percentage is obtained by Eq. (6):

$$\%S = \left[1 - \left(\frac{\delta(F-1)}{D}\right)\right] \times 100 \tag{6}$$

The maximum TMP adsorption capacity in the adsorbent is given by Eq. (7):

$$Q = \frac{C_0 \times F_m}{m_s} \int_{t=0}^{t=x} \left(1 - \frac{C}{C_0}\right) dt \tag{7}$$

The comparison between initial Mt and SnO_2–Mt was tested using only a batch adsorption system, because swelling properties of the initial Mt made it impossible to run the dynamic experiments in the columns. The batch experiments were prepared as follow: Sealed Erlenmeyer flasks that contained 100 mg of the adsorbent (initial Mt and SnO_2–Mt) and 50 mL of the pharmaceutical solution (10 mg L^{-1}) were shaken with no pH adjustment for 24 h in dark conditions. In order to evaluate the effect of visible light on the adsorption capacity of SnO_2–Mt the experimental set up was exposed to a simulated solar light source. Light illumination was sustained using a Solar Light XPS-150 Xenon lamp with an ozone-free Xenon bulb. The light source was 30 cm away from the samples. A blank sample was also tested, just the pharmaceutical solution exposure to the light at same conditions. After the tests, the remaining solutions were directly injected into a mass spectrometer Q-TRAP 4000 (Applied Biosystems) to identify photoproducts. The mass spectra (MS) were collected for m/z from 20 to 500 and operated in a positive ion mode; enhanced product ion (EPI) was used for the data acquisition. The MS parameters for the analysis were as follows: ion spray voltage – 5500 V (highest sensitivity); the collision energy and collision energy spread were 10 and 40 V, respectively; the declustering potential was at 80 V. Nitrogen was used as curtain gas (value 25 psi) and collision gas (set to high).

3. Results and discussion

3.1. Samples' characterization

Fig. 1 shows the XRD of the raw montmorillonite (Mt) and SnO_2–Mt samples. A typical diffraction peak (0 0 1) for montmorillonite clays at $2\theta = 6.6°$ corresponds to a basal spacing of 1.33 nm. After modification with tin this peak moves to a low angle at 4.1°, which correspond to a basal spacing of 2.16 nm. Similar results were found by Chen and co-workers [36]; Jalil and co-workers [8]. This result indicates that SnO_2 exists within the interlayer space of the modify clay and these species were introduced via an ion exchange process. Moreover, the XRD patterns of SnO_2–Mt show a characteristic diffraction peak for tin oxide at $2\theta = 33.8$, indicating the presence of SnO_2 crystalline particles in the modified Mt [37]. Scherrer formula for the estimation of a crystallite size was used and the crystallite size of 21 nm was found [38].

Changes in the porosity upon pillaring are reflected in a nitrogen uptake (Fig. 2). The isotherm for Mt shows a typical shape for clays with low adsorption of N_2 at low relative pressures

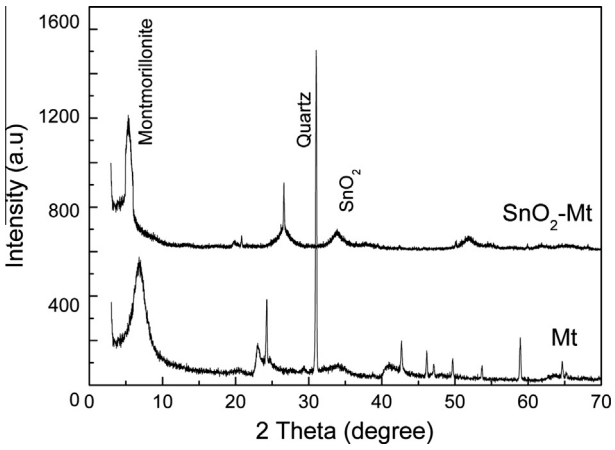

Fig. 1. XRD patterns of samples before and after modification.

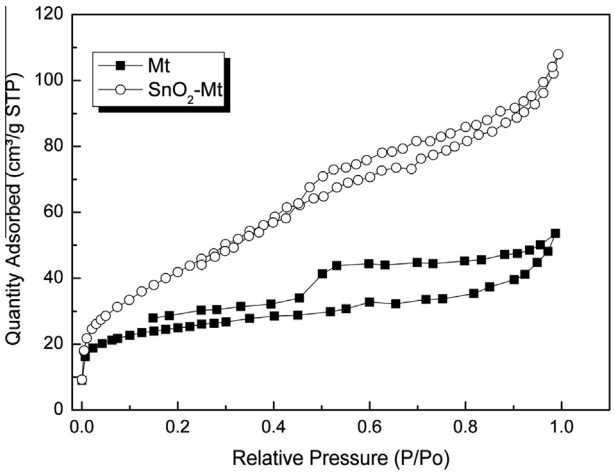

Fig. 2. N_2 adsorption–desorption isotherms at 77 K.

evidencing the small contribution of micropores to the material's structure. At higher relative pressures, larger mesopores/voids between particle aggregates are filled [8]. On the other hand, the SnO_2–Mt sample shows much higher adsorption of N_2 than Mt at low relative pressures which is linked to an increase in the volume of micropores. These micropores exist between the clay layers separated by tin oxide pillars. Moreover, the shape of the isotherms indicates that the volume of mesopores significantly increased. We link it to the precipitation of tin species onto the outer surface of clay flakes. Similar results were discussed by Petridis and Bakas [21]. They intercalated divalent tin into montmorillonite by reacting partially hydrolyzed solutions of $SnCl_2$ under aerobic conditions and used the Mosbauer analysis in order to study the dynamics of motion of tin atoms on the clay surfaces. The main conclusion from that study was that 75% of Sn^{2+} ions undergo oxidation to the +4 state with concomitant hydrolysis and condensation that led to the precipitation of SnO_2 on the external surfaces of the clay. The rest of Sn^{2+} ions were introduced into the interlayer space. Although in our case the precipitation on the outer surface of the clay flakes was also found, the XRD results discussed above suggest that only Sn^{4+} exists, either on the flakes or within the interlayer space.

X-Ray fluorescence analysis was performed to identify and quantify the elements that were present in both Mt and Mt–SnO_2. The Si/Al ratio was obtained from the weight percentage data (Table 2) of the samples, which were 8 and 9.7 for the Mt and

Table 2
Content of the elements based on XRF analysis.

Element	Mt (%)	Mt–SnO_2 (%)
Sn	–	53.6
Si	57.7	27.0
Al	7.2	2.8
Fe	29.3	13.7
Ca	2.7	–
K	0.7	–
Mn	0.1	–
Cl	0.4	1.8
Ti	1.9	1.1

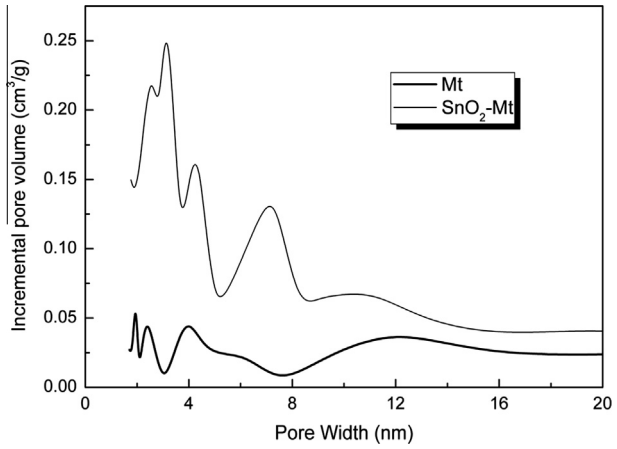

Fig. 3. Pore size distributions curves for Mt and SnO_2–Mt.

Table 3
The parameters of porous structure calculated from nitrogen adsorption isotherms.

	S_{BET} (m^2/g)	V_{mic} (cm^3/g)	V_{mes} (cm^3/g)	V_t (cm^3/g)
Mt	84	0.038	0.045	0.083
SnO_2–Mt	156	0.058	0.109	0.167

Mt–SnO_2, respectively, indicating an increase in the hydrophobicity after the pillaring process. As expected, sodium and calcium losses were observed in the Mt–SnO_2 compared to the Mt due to the exchange of those ions with the Sn species. According to the results an amount of 53.6% of tin was incorporated to the clay after pillaring process.

The isotherms for both materials exhibit hysteresis loops demonstrating the presence of mesopores, which can be classified as H4 type for the Mt and H3 type for the SnO_2–Mt [39]. The small "gap" between desorption and adsorption branches for Mt indicates the significant kinetic limitation for N_2 to enter the small pores of this material. This is linked to its very small size of the interlayer space.

Details on the porosity are also presented in Fig. 3 as pore size distributions (PSDs). The SnO_2–Mt is predominantly mesoporous with the high volume in pores with size between 2 and 5 nm. We expect these pores to have a marked effect on physical adsorption of pharmaceuticals. Similar results were found by Li and co-workers [40] who synthesized porous SnO_2-pillared tetratitanate nanocomposites. Their material was mesoporous with a gallery height of about 2 nm and a specific surface area of 154 m^2/g. Wang and co-workers [25] prepared a SnO_2–hexaniobate layered nanocomposite and also found an increased volume of mesopores upon pillaring SnO_2 nanoparticles into the interlayers.

The parameters of the porous structure calculated from N_2 isotherms are collected in Table 3. As seen, the surface area and the volume of pores for montmorillonite increased almost twice upon pillaring. The increase in the surface area and porosity must be linked not only to the pillaring process but also to the deposition of tin oxide on the outer surface of montmorillonite flakes and the aggregation of these flakes. The latter is expected to have a significant effect on the mesoporosity development.

SEM micrographs of Mt and SnO_2–Mt are shown in Fig. 4. These images reveal the variations in morphologies. The surface Mt (Fig. 4A). consists of large particle aggregates with smooth surfaces. The particles exhibit face–face and face–edge layer aggregations, which are classical arrangements for montmorillonite clays [8,36]. The SnO_2–Mt (Fig. 4B) shows less face to edge aggregations and consequently a more ordered morphology. The less smooth surface that that of Mt confirms the existence of another phase deposited on the flakes.

3.2. Analysis of the dynamic adsorption process

The experimental breakthrough curves are shown in Fig. 5. The values of the adsorption capacities, breakthrough and exhaustion volumes (chosen, respectively, as 5% and 90% of the initial concentration) are shown in Table 4. The breakthrough volume value indicate the service time of an adsorbent until first breakthrough volumes are reached, in other words, when the effluent concentration is different from zero. For SnO_2–Mt at dark conditions, the service time was 684 h, while for SnO_2–Mt exposed to solar light that time was 735 h (Table 4). For SnO_2–Mt at dark conditions, the total time to establish the PAZ (which corresponds to the zone

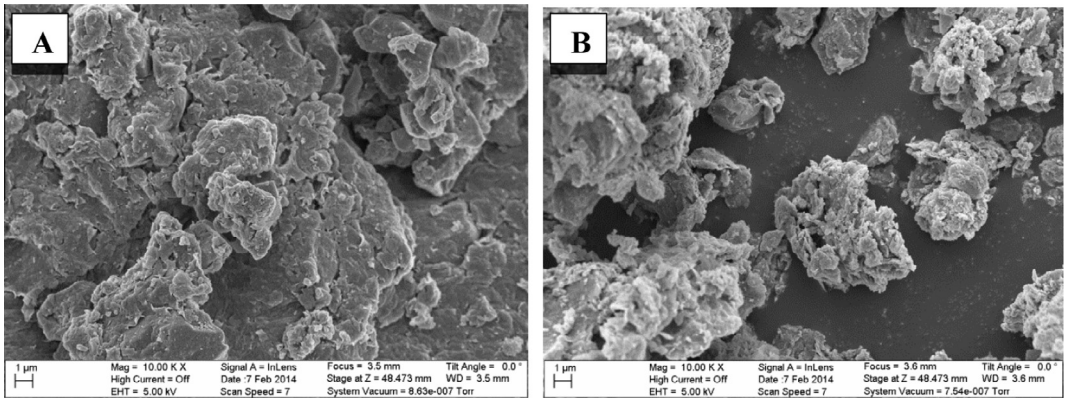

Fig. 4. SEM micrographs of Mt (A) SnO_2–Mt (B).

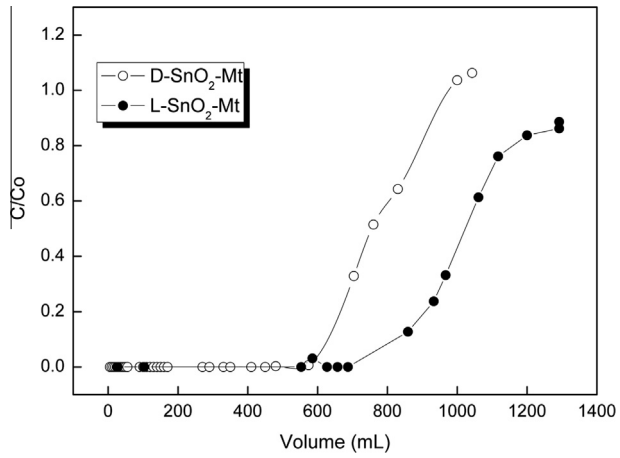

Fig. 5. Comparison of SnO_2–Mt breakthrough curves for trimethoprim measured at dark (D-SnO_2–Mt) and light (L-SnO_2–Mt) conditions.

between exhaustion point and C_b breakpoint) (t_x), was 1034.5 h, while SnO_2–Mt under solar irradiation – 1552 h. Calculations of the adsorption capacity indicate that the SnO_2–Mt under solar light exposure adsorbs 32% more TMP than in the dark (32.6 mg g^{-1} vs 24.7 mg g^{-1}) (Table 4). This indicates the photoactivity of the adsorbent and its positive effect on the performance.

Interestingly, when SMX was used as an adsorbate, the breakthrough occurred immediately for the SnO_2 modified clay. This suggests that two chosen pharmaceuticals interact with the surface of SnO_2–Mt in different ways and there are specific sites on the surface of this adsorbent, which enhance TMP retention.

3.3. Batch adsorption experiments

Since our adsorbent is able to remove efficiently only TMP, to further evaluate the effect of light on its adsorption the batch experiment were set up in the dark or under the visible light exposure. Moreover, the photolysis without the presence of the adsorbent was also tested. The latter experiments showed that exposure of the TMP solution to our solar light simulator results in 15% degradation of TMP and 57% degradation of SMX.

According to Lam and Mabury [41], the majority of the pharmaceuticals absorb little or no radiation above 290 nm, which suggests that indirect photoreactions involving ·OH could potentially contribute to their degradation. SMX was found as more susceptible to degradation by solar light than TMP. This happens because apparently the photo isomer of SMX is formed quickly after several minutes of irradiation [41]. Ryan and co-workers [42] studied the direct and indirect photolysis on SMX and TMP transformation in wastewater effluents. According to them both pharmaceuticals are susceptible to photolysis and about 48% of SMX and 18% for TMP were degraded, which agrees with our results. This may be expected, since aromatic amines mostly show little photochemical reactivity [41]. Bergh and co-workers [43] indicated that although TMP is a relatively stable drug, it is susceptible to degradation under certain conditions, such as direct sunlight. Since the direct photolysis of TMP decreases its concentration of 15%, the 32% increase in the adsorption upon light exposure compared to dark must be related not only to the direct photolysis but also to the effect of SnO_2–Mt photoactivity.

In our batch experiments in dark conditions (D-SnO_2–Mt) 0.3 mg g^{-1} of SMX was adsorbed. On the other hand, exposure to light showed that 1 g of adsorbent decreased the SMX concentration equivalent to 0.6 mg. Since a direct photolysis of SMX decreases the concentration of SMX of about 50% we conclude that the direct exposure to light does not cause any increase in the affinity of the modified sample to adsorb SMX. When adsorption of TMP was studied in the dark and under the visible light exposure, the adsorption capacity increased from 26.5 to 33 mg g^{-1} (Fig. 6). These results are very similar to those obtained in the dynamic experiments suggesting fast kinetics of the adsorption/reactive adsorption process on SnO_2–Mt.

Based on the data collected in Fig. 6 it is clearly seen that modification of montmorillonite with SnO_2 increases 5 times the

Table 4
Parameters describing the breakthrough behavior of TMP on SnO_2–Mt.

Condition	V_b	V_x	t_x[a]	t_δ[a]	t_f[a]	f[a]	% SAT	Q (mg g^{-1})
Dark	595.4	900.0	1500.00	507.7	405.7	0.201	62.9	24.7
Light	639.2	1350.0	2250.0	1184.6	741.8	0.374	50.8	32.6

[a] t_x is the time to establish PAZ (min); t_δ is the time required for movement of PAZ down the column (min); t_f is the PAZ formation time; f is the adsorbent fractional capacity in the adsorption zone.

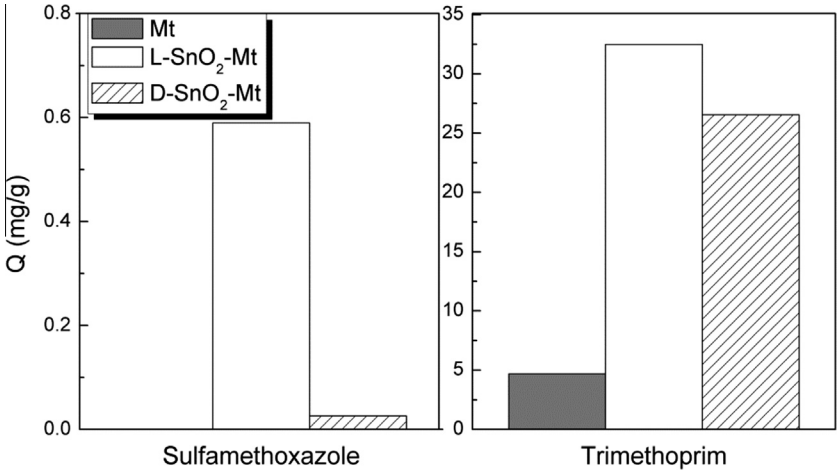

Fig. 6. Adsorption capacity for the selected samples (initial Mt, D-SnO_2–Mt, L-SnO_2–Mt). Conditions – initial concentration: 10 ppm; flow rate: 0.87 mL h^{-1}; pH: 7.

amount of TMP adsorbed in dark condition. Even for SMX a small increase from 0 to 0.03 mg g^{-1} was found. Since the porosity increased only about twice after the modification, we link such a pronounced effect of the increase in the amount of TMP adsorbed to the specific interactions of the adsorbate with the tin oxide species deposited on the surface.

In order to identify the photoactivity products, the initial solutions of SMX and TMP and those after irradiation were studied using mass spectroscopy. The molecular ion of SMX (m/z = 254) and the product ion H_2N–C_6H_4–SO_2 (m/z = 156), which is a typical fragment from sulfonamides (41; 44) were monitored. For the SMX after irradiation a low signal at m/z 99 [$C_4H_7N_2O$] appears (Fig. 2S of Supplementary Information) which arise from the cleavage of the bond between the aminophenylsulfone and the methylisoxazoleamine moieties [44]. Except for the m/z 99, the two spectra are almost identical. Similar results are found by Lam and Mabury [41]. According to them, the photoisomerization of the isoxazole ring of SMX leads to the formation of its major degradation product 4-amino-N-(5-methyl-2-oxazolyl)benzenesulfonamide after several minutes. This imido tautomeric form of the parent compound is identical in mass to SMX compound.

On the spectra for TMP after irradiation new species with m/z = 307 and m/z = 155 appear (Fig. 3 of Supplementary Information). Similar results were obtained by Michael and co-workers [45], who studied the solar photocatalytic treatment of TMP in four environmental matrices. According to them, the major changes generated during the photocatalysis occur in the trimethoxybenzyl moiety. They found two photoproducts of the TMP cleavage: $C_5H_7N_4O$ (m/z = 139) and $C_5H_7N_4O_2$ (m/z = 155). They also suggested that hydroxylation reactions results in two distinct monohydroxylated products, corresponding to the addition of 16 mass units to the TMP molecule (m/z = 307, $C_{14}H_{19}N_4O_4$). Apparently a direct photolysis of TMP results in more polar degradation products with a significant content of oxygen.

Bekçi and co-workers [46] investigated montmorillonite as an adsorbent in the removal of trimethoprim. Results showed that the process was exothermic because the adsorption efficiency increased with a decrease in the temperature. As a consequence of thermodynamic studies, the authors demonstrated that physisorption was the main adsorption mechanism. Another parameter that affected trimethoprim adsorption was pH. At low pH conditions (in an aqueous solution montmorillonite has a pH value of 3.31), trimethoprim is in the protonated form, so it was strongly adsorbed to the negatively charged surface of the montmorillonite. In the best conditions, the amount of drug adsorbed was 60 mg g^{-1} for 1 h of a contact time (initial compound concentration was 290.3 mg L^{-1}). This amount is much higher than that obtained in our experiments and the discrepancy can be explained by the fact that a higher initial concentration of adsorbate tends to enhance the adsorption capacity.

Domınguez-Vargas and co-workers [47] studied the removal of trimethoprim from water using Resin Amberlite XAD-7 (an acrylic ester polymer exhibiting an intermediate value of polarity and a moderately hydrophilic behavior) as an adsorbent. They found a 70% removal efficiency in the first 2 h with adsorption capacity of 15.88 mg g^{-1} (the initial concentration was 75 mg L^{-1}).

The adsorption of trimethoprim on powdered activated carbon (PAC) and granular activated carbon (GAC) was studied by Kim and co-workers [29]. The rate of adsorption on these materials was rapid and the equilibrium state was reached after 30 min with 100 rpm. However, separation of PAC from aqueous solution was not easy and GAC application was suggested. The adsorption capacity on the former sample was about 200 mg g^{-1} for PAC and for the latter 50 mg g^{-1} with the initial concentration of 50 mg L^{-1}. This leads to the conclusion that our material has comparable affinity to adsorb TMP than that found on granular activated carbon used by Kim and co-workers [29].

3.4. Analysis of the adsorption mechanism

In order to formulate the hypothesis why our modified clay is a good adsorbent for TMP and why visible light exposure helps with this, the chemistry of the surface of the initial adsorbent and that after adsorption in the dynamic conditions was analyzed. Fig. 7 shows the infrared spectra of the Mt; SnO_2–Mt; D-SnO_2–Mt–TMP and L-SnO_2–Mt–TMP. The band of Mt at 1634 cm^{-1} is attributed to the OH deformation vibration of water, and 1000 cm^{-1} is assigned to Si–O stretching vibration [48]. The bands at 534 and 669 cm^{-1} are assigned to Sn–O stretching vibration of Sn–OH and Sn–O–Sn [49], whereas these ones at 799 and 776 cm^{-1} could be due to the bending of O–Sn–O [49,50]. The spectrum of the exhausted samples is basically the same as the spectrum of SnO_2–Mt. According to Bekçi and co-authors [47] the bands linked to the trimethoprim should be expected at 1632 and 1590 cm^{-1}. The weak bands at these wavelengths are seen on the spectra for the exhausted samples, especially for that exposed to light.

The surface pH_{pzc} values were evaluated from titration curves. These curves are show in Fig. 8, where the pH_{pzc} value corresponds to the pH where the curve crosses the x-axis (ϑ = 0). The values obtained were 8.8, 3.3; 6.3 and 6.9 for the Mt, SnO_2–Mt; D-SnO_2–Mt–-TMP and L-SnO_2–Mt–TMP, respectively. It shows that upon pillaring a significant acidification of the surface occurred likely due to the introduction of tin species of an acidic character to the SnO_2–Mt sample. After TMP adsorption the samples (D-SnO_2–Mt–TMP and L-SnO_2–Mt–TMP) become more basic suggesting an involvement of acidic sites in the adsorption process. SnO_2–Mt exposed to visible light is more basic than D-SnO_2–Mt–TMP. We linked it to more TMP adsorbed and, if exposure to light promotes the oxidation of TMP, these oxidized species could have the higher affinity to water than to the clay surface.

The Bronsted and Lewis acidity of pillared clays is related to the properties of the mineral layers as well as the acidic centers introduced in the form of pillars [51]. It is known that when pillars are composed of metal oxides or hydroxides such as hydroxy-aluminum or hydroxy-zirconium poly- cations, the acidic properties of the clay

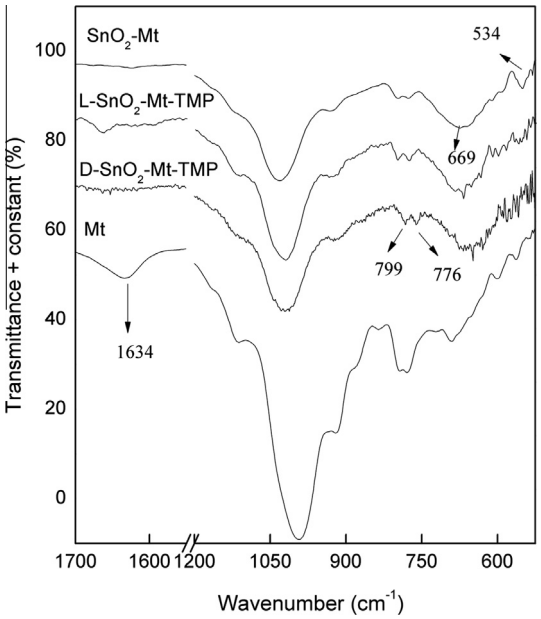

Fig. 7. FTIR spectra for the initial and exhausted samples.

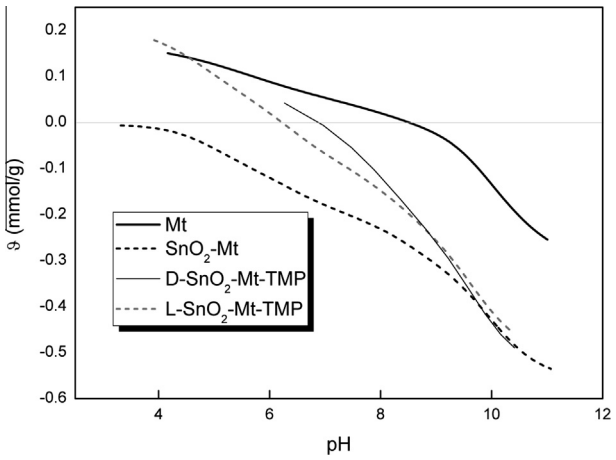

Fig. 8. Potentiometric titration curves of the Mt; SnO_2–Mt; D-SnO_2–Mt–TMP and L-SnO_2–Mt–TMP.

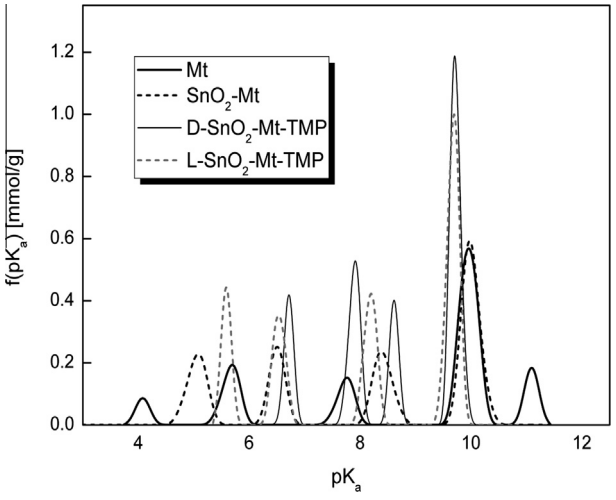

Fig. 9. pK_a distributions for Mt, SnO_2–Mt; D-SnO_2–Mt–TMP and L-SnO_2–Mt–TMP. Conditions: 0.01 M $NaNO_3$ electrolyte.

surface are enhanced [51]. In this work, the same behavior was observed using tin oxide as the pillars.

The pK_a distribution of the species present on the surface of the Mt sample reveals five peaks (Fig. 9). Since the reports published in the literature indicate that acidic sites in montmorillonite have pK_a values of 5.6 and 8.2 [52–56], the pK_as found on our sample at 5.67 and 7.74 are in agreement with those results. The first peak at pK_a 4.07 can be assigned to bridging OH groups linked to a tetrahedral or/and an octahedral aluminum cations and the third peak (pK_a 7.74) corresponds to terminal OH groups coordinated to a single tetrahedral Al^{3+} cation [51]. The second peak, at pK_a 5.67 can be assigned to the presence of silanol groups. The fourth peak at pK_a 9.96 represents weaker acidity associated to the bridging of siloxane groups [51]. The fifth peak can be assigned (pK_a 11.09) to water molecules in interlayer space of clay. According to Bergaya and co-workers [57] and Liu and co-workers [58] the water molecules in an interlayer space of clay minerals can accept a pair of electrons and thus serve as the major Lewis acid sites. They can show a pK_a value around 11.5. Nevertheless, up to now the absolute acidities of confined waters and the confinement effects of clay pores have not been revealed clearly. In SnO_2–Mt and SnO_2–Mt–TMP there is no presence of this peak, since these samples do not have water in their interlayer space, owing to the calcination step in the pillaring process leading the surface hydrophobicity.

In the case of the SnO_2–Mt, a shift in the positions of the first and second peaks to higher pK_a (4.86 and 6.41, respectively) is found in comparison with the initial clay. This is also accompanied by a significant increase in the number of groups represented by these species. Following the history of this sample, its stronger acidity is linked to the presence of tin oxide on the surface and the protonation of its oxygen sites by water. Gyftopoulou and co-workers [13] studied tin pillared clays as catalysts for hydrocracking of heavy liquid fuels. They found that the incorporation of tin-oxide to the clay's acidic sites is responsible for the hydrocracking activity, which is usually attributed to higher surface acidity. Interestingly, in comparison with the initial clay the numbers of weakly acidic groups associated to bridging siloxane groups decreased which might suggest interactions of SnO_2 species with the bridging oxygen of SiO_2 layers.

After trimethoprim adsorption, the number of all acidic sites significantly increases (Table 5) with a slight shift to higher acidity. This could be related to the protonated NH_2 species present in the TMP compound. This is a direct indication of TMP adsorbed and of its strong interactions with the surface sites.

TG and DTG curves for Mt, SnO_2–Mt, D-SnO_2–Mt–TMP and L-SnO_2–Mt–TMP are shown in Fig. 10. For Mt, the major weight loss, about 6%, occurs below 200 °C, corresponding to the removal of physically adsorbed water. For SnO_2–Mt, the weight loss in this temperature range was relatively small, about 2%, owing to the calcination applied during its synthesis. Above 500 °C, the weight loss is attributed to the dehydroxylation of the clay and pillars [36].

For exhausted samples, the complex peaks representing weight loss with maxima at 650 and 750 °C are linked to the removal of TMP compound (boiling point of 530 °C). The peak at 750 °C may also include the products of TMP oxidation. They have higher boiling points than the parent compounds. Similar results were found by Fernandes and co-workers [59]. They also observed two peaks of TMP decomposition between 240 and 700 °C.

Even though the similar weight loss patterns are found for the both exhausted samples, more species are thermally desorbed from the surface of the SnO_2–Mt exposed to visible light. This is linked to the higher adsorption capacity for TMP than that in the dark. Moreover, a marked increase in the intensity of the high temperature peak suggests the higher extent of TMP conversion on the surface of this material when exposed to visible light compared to its activity in the dark.

More details are provided from MS analysis of the thermal decomposition products from the surface of SnO_2–Mt exposed to TMP in either dark or light (Fig. 11). The initial and exhausted

Table 5
Results of potentiometric titration: peak positions and numbers of groups (in parentheses; [mmol/g]).

Sample	pH[a]	pK_a 4–5	pK_a 5–6	pK_a 6–7	pK_a 7–8	pK_a 8–9	pK_a 9–10	pK_a 10–11	All
Mt	7.7	4.07 (0.028)	5.67 (0.08)		7.74 (0.060)		9.96 (0.251)	11.09 (0.061)	0.480
SnO_2–Mt	4.2	4.86 (0.12)		6.41 (0.117)		8.40 (0.068)	9.68 (0.168)		0.477
D-SnO_2 TMP	5.5		5.59 (0.10)	6.54 (0.111)		8.18 (0.13)	9.68 (0.283)		0.625
L-SnO_2 TMP	6.2			6.71 (0.09)	7.90 (0.14)	8.61 (0.09)	9.72 (0.29)		0.610

[a] Initial pH of the clays suspension used for titration.

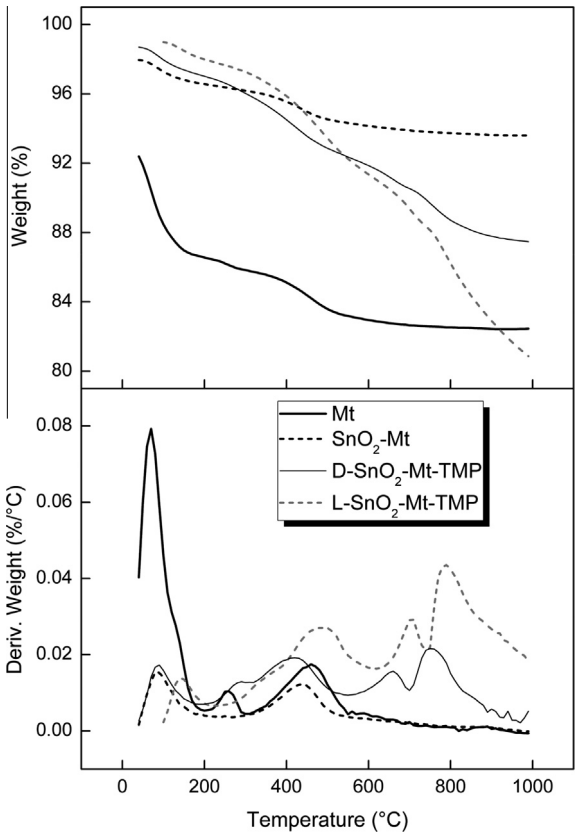

Fig. 10. TG and DTG curves for Mt, SnO_2–Mt and SnO_2–Mt–TMP.

samples show differences in the thermal patterns for m/z 18 linked to the removal of water. The peaks for the exhausted samples are more complex than for the initial one and especially for the sample exposed to TMP in the dark. Apparently, the condensation reactions of TMP with surface OH groups, as suggested from potentiometric titration data, might contribute to this behavior. After TMP adsorption the thermal desorption patterns for m/z 44 profiles agree with the major weight loss over 500 °C. They likely represent the removal of the primary amides (O=C=NH_2) from decomposition of TMP compounds [60]. Complex removal of hydrogen ($m/z = 2$) must be also related to the thermal transformation of adsorbed TMP. The m/z 16 profile is linked to the removal of oxygen (for the initial sample) or oxygen and NH_2 from the samples with adsorbed TMP and its decomposition products. As seen, the intensity of the peaks on this profile over 350 °C increases after adsorption, and especially for the sample exposed to light which is in agreement with the high amount of TMP adsorbed on this sample. Differences in the m/z profiles between the sample exposed to light and dark are mainly in higher intensities of the high temperature peaks for the former sample. This might be due to the presence of the decomposition products of TMP in the very small pores of the interlayer space. Removal of these species requires more energy than when the same species are present in the pores of larger sizes.

Based on the results discussed above, the higher affinity of SnO_2–Mt to adsorb TMP than that of the unmodified clay is linked to the introduction of acidic groups in the form of SnO_2 and the formation of porosity, either between the clay layers of between the SnO_2 particles deposited on the outer surfaces of the clay flakes. Owing the presence of NH_2 moieties and piridinic nitrogen (Lewis bases) these species are strongly interacting with the acidic groups arising from the presence of the SnO_2 phase (Lewis acids). This causes a significant decrease in surface acidity after the adsorption

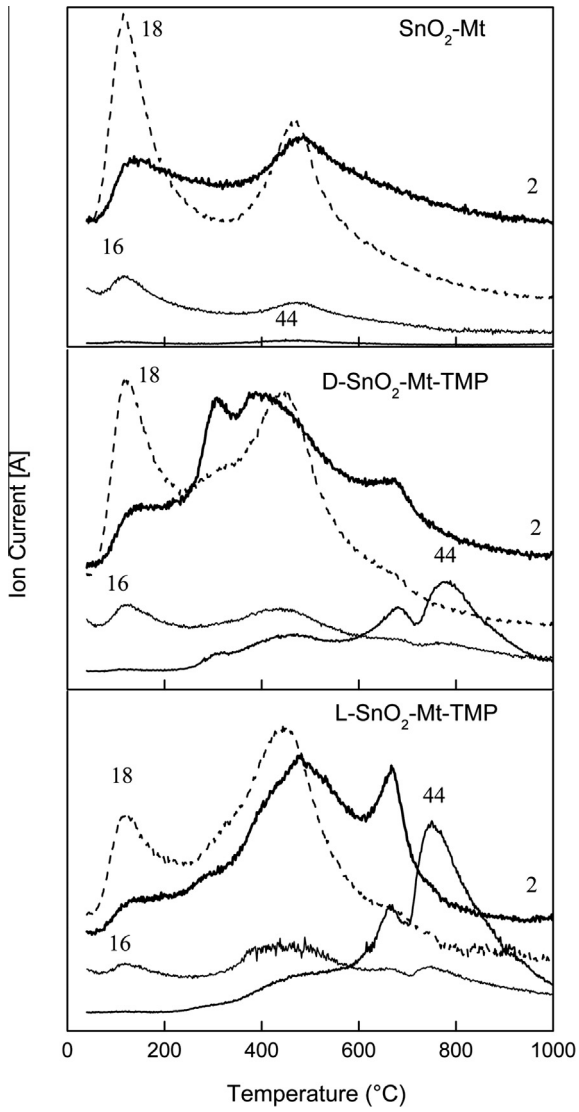

Fig. 11. Mass spectra for SnO_2–Mt, D-SnO_2–Mt–TMP and L-SnO_2–Mt–TMP.

process. Not without importance is the linear shape of TMP molecule and thus the high probability that it enters the expanded interlayer space after the pillaring process.

To explain why our adsorbent show no activity for the SMX retention, the differences in the polarity, chemistry and the shape of molecules should be taken into account. The first factor might play a paramount role promoting stronger interactions of SMX with the solvent than with the relatively hydrophobic after calcination surface of the clay decorated with the SnO_2 particles. The more geometrically complex shape of SMX molecule than that of TMP can limit the access for the former species to the interlayer space of the modified clay. The acidic character of SMX might also result in rather repulsive interactions of this molecule with the acidic surface of SnO_2–Mt. Since the pK_as values of SMX are less than 7 at the pH of our experiments (about 7.5) this species exists in a deprotonated form. Owing to the negatively charged surface at this pH, electrostatic interactions are not expected to play any role in the adsorption process. On the other hand, these interactions can enhance the TMP adsorption.

An explanation of an increase in the amount adsorbed of TMP upon the visible light irradiation might be in the surface oxidation of adsorbed TMP molecules owing to the photoactivity of SnO_2. It is likely that formed OH radicals on the surface of the adsorbent oxidize TMP to form smaller more polar species [45]. They are able to

enter the pores which are not accessible for TMP. This process results in releasing the active centers for adsorption of more TMP molecules from the solution via acid base and electrostatic interactions. The possible molecules formed on the surface as a result of photoactivity are two photoproducts: $C_5H_7N_4O$ (m/z = 139) and $C_5H_7N_4O_2$ (m/z = 155) found on MS spectra after direct photolysis.

4. Conclusions

The Brazilian clay modified by the incorporation of tin oxide via the pillaring process showed an enlargement of the clay's interlayer space and an enhancement in the volume of mesopores. This indicates that the SnO_2 particles were not only intercalated within the clay interlayer space but also precipitated on the outer surface of clay flakes. The SnO_2–Mt sample showed an increase in TMP adsorption capacity compared to the unmodified clay and when solar simulated light was used in the adsorption process. This effect was linked to the specific acid–base and electrostatic interactions of TMP with the Lewis acid sites of SnO_2. An increase in TMP adsorption in visible light was linked to trimethoprim oxidation/degradation on the clay surface as a result of its photoactivity. The attraction of the formed decomposition products to small pores resulted in releasing additional centers for TMP reactive adsorption. The SMX was not adsorbed on the surface of SnO_2 modified clay owing to the acidic character of the adsorbent and adsorbate.

Acknowledgements

CBV would like to thank Brazil Science Without Borders Graduate Program (*Ciências sem Fronteiras*) and CAPES (Coordination of Higher Level Personal Improvement) for the scholarship and financial support – Process: CSF SDW 10568/13-1. This publication was also made possible owing a partial support by USEPA grant (RD835178). Its contents are solely the responsibility of the grantee and do not necessarily represent the official views of the USEPA. Further, USEPA does not endorse the purchase of any commercial products or services mentioned in the publication.

Appendix A. Supplementary data

Supplementary data associated with this article can be found, in the online version, at http://dx.doi.org/10.1016/j.cej.2014.07.079.

References

[1] K. Fent, A.A. Weston, D. Caminada, Ecotoxicology of human pharmaceuticals, Aquat. Toxicol. 76 (2006) 122–159.
[2] C.B. Vidal, G.P. Pessoa, A.V. Feitosa, G.S.C. Raulino, A.G. Oliveira, A.B. Santos, R.F. Nascimento, Polymeric and silica sorbents on endocrine disruptors determination, Desalination Water Treat. (2014) 1–10.
[3] J. DeRudder, T. Van de Wiele, W. Dhooge, F. Comhaire, W. Verstraete, Advanced water treatment with manganese oxide for the removal of 17α-ethinyl estradiol (EE2), Water Res. 38 (2004) 184–192.
[4] S. Fukahori, T. Fujiwara, R. Ito, N. Funamizu, PH-dependent adsorption of sulfa drugs on high silica zeolite: modeling and kinetic study, Desalination 275 (2011) 237–242.
[5] G.P. Pessoa, A.B. dos Santos, N.C. Souza, J.A.C. Alves, R.F. Nascimento, Development of methodology to determine estrogens in wastewater treatment plants, Quim. Nova 35 (2012) 968–973.
[6] G. Rytwo, S. Nir, M. Crespin, L. Margulies, Adsorption and interactions of methyl green with montmorillonite and sepiolite, J. Colloid Interface Sci. 222 (2000) 12–19.
[7] J. Wu, B. Li, J. Liao, Y. Feng, D. Zhang, J. Zhao, W. Wen, Y. Yang, N. Liu, Behavior and analysis of Cesium adsorption on montmorillonite mineral, J. Environ. Radioact. 100 (2009) 914–920.
[8] M.E.R. Jalil, R.S. Vieira, D. Azevedo, M. Baschini, K. Sapag, Improvement in the adsorption of thiabendazole by using aluminium pillared clays, Appl. Clay Sci. 71 (2013) 55–63.
[9] G.W. Brindley, C.-C. Kao, Formation, compositions and properties of hyrdroxy-Al- and hydroxy-Mg-montmorillonite, Clay Clay Miner. 28 (1980) 435–443.
[10] T.J. Pinnavaia, Intercalated clay catalysts, Science 220 (1983) 365–371.
[11] Z. Ding, J.T. Kloprogge, R.L. Frost, Porous clays and pillared clays-based catalysts. Part 2: a review of the catalytic and molecular sieve applications, J. Porous Mater. 8 (2001) 273–293.
[12] A. Gil, S.A. Korili, R. Trujillano, M.A. Vicente, A review on characterization of pillared clays by specific techniques, Appl. Clay Sci. 53 (2011) 97–105.
[13] M.E. Gyftopoulou, M. Millan, A.V. Bridgwater, D. Dugwell, R. Kandiyoti, J.A. Hriljac, Pillared clays as catalysts for hydrocracking of heavy liquid fuels, Appl. Catal. A Gen. 282 (2005) 205–214.
[14] A. Sharma, A.P. Singh, P. Thakur, N.B. Brookes, S. Kumar, C.G. Lee, R.J. Choudhary, K.D. Verma, R. Kumar, Structural, electronic, and magnetic properties of Co doped SnO_2 nanoparticles, J. Appl. Phys. 107 (2010) 1–7.
[15] A. Sharma, M. Varshney, K.D. Verma, Y. Kumar, R. Kumar, Structural and surface microstructure evolutions in SnO thin films underion irradiation, Nucl. Instrum. Methods B 308 (2013) 15–20.
[16] I.T. Weber, A. Valentini, L.F.D. Probst, E. Longo, E.R. Leite, Influence of noble metals on the structural and catalytic properties of Ce-doped SnO_2 systems, Sens. Actuators B Chem. 97 (2004) 31–38.
[17] S.P. Mondal, S.K. Ray, J. Ravichandran, I. Manna, Temperature dependent growth and optical properties of SnO_2 nanowires and nanobelts, Bull. Mater. Sci. 33 (2010) 357–364.
[18] F. Mendoza, D.M. Hernández, V. Makarov, E. Febus, B.R. Weiner, G. Morell, Room temperature gas sensor based on tin dioxide-carbon nanotubes composite films, Sens. Actuators B Chem. 190 (2014) 227–233.
[19] F.J. Berry, M.S. Beevers, S.P. Bond, W.R. McWhinnie, Tin-119 mossbauer spectroscopic studies of novel tin oxide pillared clays, Hyperfine Interact. 68 (1991) 181–184.
[20] I. Hannus, I. Palink, K. Lázár, J.B. Nagy, I. Kiricsi, The chemical state of Sn in Sn-montmorillonite; A multinuclear MAS NMR and ^{119}Sn Mossbauer spectroscopic study, J. Mol. Struct. 349 (1995) 179–182.
[21] D. Petridis, T. Bakas, Tin–clay complexes: a mossbauer study, Clay Clay Miner. 45 (1997) 73–76.
[22] M. Batzill, U. Diebold, The surface and materials science of tin oxide, Prog. Surf. Sci. 79 (2005) 47–154.
[23] H. Yuan, J. Xu, Preparation, characterization and photocatalytic activity of nanometer SnO_2, Int. J. Chem. Eng. Appl. 1 (2010) 241–246.
[24] H. Seema, K.C. Kemp, V. Chandra, K.S. Kim, Graphene–SnO_2 composites for highly efficient photocatalytic degradation of methylene blue under sunlight, Nanotechnology 23 (2012) 1–8.
[25] Q.Q. Wang, B.Z. Lin, B.H. Xu, X.L. Li, Z.J. Chen, X.T. Pian, Preparation and photocatalytic properties of mesoporous SnO_2–hexaniobate layered nanocomposite, Micropor. Mesopor. Mater. 130 (2010) 344–351.
[26] J. Bandara, K. Tennakone, P.P.B. Jayatilaka, Composite tin and zinc oxide nanocrystalline particles for enhanced charge separation in sensitized degradation of dyes, Chemosphere 49 (2002) 439–445.
[27] M. Zhang, G. Sheng, J. Fu, T. An, X. Wang, X. Hu, Novel preparation of nanosized ZnO–SnO_2 with high photocatalytic activity by homogeneous co precipitation method, Mater. Lett. 59 (2005) 3641–3644.
[28] F. Fresno, C. Guillard, J.M. Coronado, J.M. Chovelon, D. Tudela, J. Soria, J.M. Herrmann, Photocatalytic degradation of a sulfonylurea herbicide over pure and tin-doped TiO_2 photocatalysts, J. Photochem. Photobiol. A 173 (2005) 13–20.
[29] J. Kim, J.S. Lee, M. Kang, Synthesis of nanoporous structured SnO_2 and its photocatalytic ability for bisphenol destruction, B. Korean Chem. Soc. 32 (2011) 1715–1720.
[30] C.B. Vidal, G.S.C. Raulino, A.L. Barros, A.C.A. Lima, J.P. Ribeiro, M.J.R. Pires, R.F. Nascimento, BTEX removal from aqueous solutions by HDTMA-modified Y zeolite, J. Environ. Manage. 112 (2012) 178–185.
[31] M. Seredych, T.J. Bandosz, Removal of dibenzothiophenes from model diesel fuel on sulfur rich activated carbons, Appl. Catal. B Environ. 106 (2011) 133–141.
[32] J. Jagiello, T.J. Bandosz, J.A. Schwarz, Carbon surface characterization in terms of its acidity constant distribution, Carbon 32 (1994) 1026–1028.
[33] J. Jagiello, Stable numerical solution of the adsorption integral equation using splines, Langmuir 10 (1994) 2778–2785.
[34] C. Contescu, J. Jagiello, J.A. Schwarz, Heterogeneity of proton binding sites at the oxide/solution interface, Langmuir 9 (1993) 1754–1765.
[35] D.O. Cooney, Adsorption Design for Wastewater Treatment, CRC Press, Boca Raton, Florida, USA, 1999.
[36] D. Chen, G. Du, Q. Zhu, F. Zhou, Synthesis and characterization of TiO_2 pillared montmorillonites: application for methylene blue degradation, J. Colloid Interface Sci. 409 (2013) 151–157.
[37] M. Klementová, M. Rieder, Z. Weiss, Rietveld refinement of cassiterite: a caveat for meticulous sample preparation, J. Czech Geol. Soc. 45 (2000) 155–157.
[38] J.I. Langford, J.C. Wilson, Scherrer after sixty years: a survey and some new results in the determination of crystallite size, J. Appl. Cryst. 11 (1978) 102–113.
[39] K.S.W. Sing, D.H. Everett, R.A.W. Haul, L. Moscou, R.A. Pierotti, J. Rouquerol, T. Siemienewska, Reporting physisorption data for gas–solid systems, Pure Appl. Chem. 57 (1985) 603–619.
[40] B. Li, B.Z. Lin, O. Zhang, L.M. Fu, H. Liu, Y.L. Chen, B.F. Gao, Heterostructured tin oxide-pillared tetratitanate with enhanced photocatalytic activity, J. Colloid Interface Sci. 386 (2012) 1–8.
[41] M.W. Lam, S.A. Mabury, Photodegradation of the pharmaceuticals atorvastatin, carbamazepine, levofloxacin, and sulfamethoxazole in natural waters, Aquat. Sci. 67 (2005) 177–188.

[42] C.C. Ryan, D.T. Tan, W.A. Arnold, Direct and indirect photolysis of sulfamethoxazole and trimethoprim in wastewater treatment plant effluent, Water Res. 45 (2011) 1280–1286.
[43] J.J. Bergh, J.C. Breytenbach, P.L. Wessels, Degradation of trimethoprim, J. Pharm. Sci. 78 (1989) 348–350.
[44] A.G. Trovó, R.F.P. Nogueira, A. Aguera, C. Sirtori, A.R. Fernández-Alba, Photodegradation of sulfametoxazole in various aqueous media: persistence, toxicity and photoproducts assessment, Chemosphere 77 (2009) 1292–1298.
[45] I. Michael, E. Hapeshi, V. Osorio, S. Perez, M. Petrovic, A. Zapata, S. Malato, D. Barceló, D. Fatta-Kassinos, Solar photocatalytic treatment of trimethoprim in four environmental matrices at a pilot scale: transformation products and ecotoxicity evaluation, Sci. Total Environ. 430 (2012) 167–173.
[46] Z. Bekçi, Y. Seki, M.K. Yurdakoc, A study of equilibrium and FTIR, SEM/EDS analysis of trimethoprim adsorption onto K10, J. Mol. Struct. 827 (2007) 67–74.
[47] J.R. Domınguez-Vargas, T. Gonzalez, P. Palo, E.M. Cuerda-Correa, Removal of carbamazepine, naproxen, and trimethoprim from water by amberlite XAD-7: a kinetic study, Clean Soil Air Water 41 (2013) 1052–1061.
[48] M.E. Parolo, M.J. Avena, G. Pettinari, I. Zajonkovsky, J.M. Valles, M.T. Baschini, Antimicrobial properties of tetracycline and minocycline-montmorillonites, Appl. Clay Sci. 49 (2010) 194–199.
[49] V. Kumar, A. Govind, R. Nagarajan, Optical and photocatalytic properties of heavily F-–doped SnO_2 nanocrystals by a novel single-source precursor approach, Inorg. Chem. 50 (2011) 5637–5645.
[50] K. Nakamoto, Infrared and Raman Spectra of Inorganic and Coordination Compounds, John Wiley & Sons, New York, 1986.
[51] T.J. Bandosz, C. Lin, J.A. Ritter, Porosity and surface acidity of SiO_2–Al_2O_3 xerogels, J. Colloid Interface Sci. 198 (1998) 347–353.
[52] H.A. Benesi, Acidity of catalyst surfaces–I: acid strength from colors of absorbed indicators, J. Amer. Chem. Soc. 78 (1956) 5490–5494.
[53] H.A. Benesi, Acidity of catalyst surfaces–II: amine titration using Hammett indicators, J. Phys. Chem. 61 (1957) 970–973.
[54] G.W. Bailey, J.L. White, T. Rothberg, Adsorption of organic herbicides by montmorillonite: role of pH and chemical character of adsorbate, Soil Sci. Soc. Am. Proc. 32 (1968) 222–234.
[55] A.E. Hirschler, A. Schneider, Acid strength distribution studies of catalyst surfaces, J. Chem. Eng. Data 6 (1961) 313–318.
[56] D.H. Solomon, J.D. Swift, A.J. Murphy, The acidity of clay minerals in polymerization and related reactions, J. Macromol. Sci. Chem. 5 (1971) 587–601.
[57] F. Bergaya, B.G.K. Theng, G. Lagaly, Handbook of Clay Science, Elsevier, Amsterdam, 2006.
[58] X. Liu, X. Lu, R. Wang, E.J. Meijer, H. Zhou, Acidities of confined water in interlayer space of clay minerals, Geochim. Cosmochim. Acta 75 (2011) 4978–4986.
[59] N.S. Fernandes, M.A.S. Carvalho Filho, R.A. Mendes, M. Ionashiro, Thermal decomposition of some chemotherapic substances, J. Braz. Chem. Soc. 10 (1999) 459–462.
[60] F.W. McLafferty, D.B. Stauffer, Wiley/NBS Registry of Mass Spectral Data, Wiley, Chichester, 1989.